Korean J. Chem. Eng., 40(12), 2839-2846 (2023)
DOI: 10.1007/s11814-023-1529-5

pISSN: 0256-1115
eISSN: 1975-7220

Optimization of the molecular weight range of coating pitch and its effect on graphite anodes for lithium-ion batteries

Ji Hong Kim*,‡, Bo Ra Kim*,,‡, and Ji Sun Im*,***,†**

*C1 Gas & Carbon Convergent Research Center, Korea Research Institute of Chemical Technology (KRICT), Daejeon 34114, Korea
**Department of Chemical Engineering and Applied Chemistry, Chungnam National University, Daejeon 34134, Korea
***Advanced Materials and Chemical Engineering, University of Science and Technology (UST), Daejeon 34113, Korea
(*Received 12 February 2023 • Revised 25 June 2023 • Accepted 10 July 2023*)

Abstract−This study aimed to optimize the molecular weight range of coating pitch to enhance the electrochemical performance of graphite-based anodes used in lithium-ion batteries by understanding the characteristics of the coating pitch. The coating pitch was divided into four fractions based on its solubility in hexane, acetone, toluene, and n-methyl-2-pyrrolidone (NMP). These four fractions were estimated based on the thickness and homogeneity of the coated surfaces. The lighter fractions of pitch, such as hexane and acetone, assisted in forming a homogeneous surface by decreasing the viscosity during carbonization. Heavy fractions, such as toluene and NMP, were the main components of the coating. They improved the rate performance of the anode by forming an isotropic layer, which increased the number of lithium-ion intercalation sites. However, thick surfaces increased the charge-transfer resistance because of the increased diffusion path lengths of lithium ions. The pitch molecular weight fractions of 128-768, 768-1152, and 1,152-1,480 m/z should be controlled to 70-84.49, 11.20-18.21, and 3.35-5.15%, respectively. Furthermore, the results of this study can be applied to optimize the coating properties for other anode materials, such as silicon, at a controllable pitch coating thickness according to the molecular weight.

Keywords: Petroleum Pitch, Molecular Weight Range, Pitch Coating, Graphite Anode, Lithium-ion Batteries

INTRODUCTION

Lithium-ion batteries (LIBs) are widely used in small-scale devices, such as portable electronics, and in large-scale applications, such as electric vehicles and energy storage systems [1-4]. As the demand for LIBs has recently increased owing to environmental regulations, battery materials have been widely studied to improve their characteristics. Among them, graphite, which is used as a commercial anode material, has been increasingly studied [5,6]. Graphite has many advantages, such as a low and constant potential, which is similar to that of lithium metal, high electrical conductivity, low price, and a stable intercalation mechanism [6-9]. However, it also has many disadvantages, such as a low initial coulombic efficiency due to the formation of a solid electrolyte interphase (SEI) layer and poor rate performance. To compensate, many researchers have found that graphite surface modifications, such as doping, oxygen treatment, and carbon coating, can improve the electrochemical properties of graphite [10-17]. Among them, carbon coating is expected to have two major effects, namely, increasing the initial coulombic efficiency and promoting the rate performance [18-21]. The edge planes of graphite have higher active energies than their basal planes, resulting in more SEI layers on the edge planes [22]. The carbon coating forms a uniform surface and prevents electrolyte decomposition on the edge plane, thereby inhibiting the formation of an SEI layer and increasing the initial Coulombic efficiency [23,24]. Additionally, the carbon coating layer forms a diffusion path for lithium ions, which facilitates lithium-ion intercalation/deintercalation and improves the rate performance [25].

Pitch is a promising coating material owing to its low cost and structural stability. It is composed of polycyclic aromatic hydrocarbons (PAHs) with molecular weights of 100-2,000 m/z. Depending on the molecular weight range of the pitch, characteristics such as the H/C atomic ratio, carbon yield, softening point, and aromaticity vary [26-30]. Furthermore, the molecular weight range of pitch can have many effects on the coating and electrochemical properties. Therefore, it is necessary to optimize the molecular weight range of coating pitch.

This study aimed to optimize the molecular weight range of coating pitch to enhance the electrochemical performance of graphite-based anodes used in LIBs by understanding the characteristics of the coating pitch. The molecular weight range of coating pitch was controlled to determine its effect on the graphite anode material of LIBs, and the molecular weight range of the coating pitch with the best electrochemical performance was considered. The molecular weight of the coating pitch was controlled by solvent extraction with four organic solvents: hexane, acetone, toluene, and n-methyl-2-pyrrolidone (NMP). The coating properties of the prepared pitch were observed based on the carbonization behavior and the effect of the surface morphology was investigated using thermal gravimetric analyses (TGA) and scanning electron microscopy (SEM), respectively. The effects of the electrochemical properties of the pitch-coated graphite anode were estimated based on the initial Coulombic effi-

†To whom correspondence should be addressed.
E-mail: jsim@krict.re.kr
‡J. H. Kim and B. R. Kim contributed equally to this work.

ciency and rate performance. The results of this study are expected to be applied to optimize the coating properties of other anode materials, such as silicon, by controlling the pitch coating thickness according to the molecular weight.

EXPERIMENTAL

1. Sample Preparation

A petroleum pitch (softening point of 255 °C; supplied by Rutgers Infratec GmbH) was used as a precursor. The molecular-weight-controlled pitch was prepared by solvent extraction, and the soluble/insoluble fraction of the pitch was measured three times using various organic solvents to determine the appropriate molecular weight. Hexane, acetone, and toluene were selected because of their different soluble/insoluble fraction ranges and small standard deviations; the results are shown in Fig. 1. NMP was also used, although its standard deviation was relatively large because the soluble fractions exceeded 90%. Dichloromethane (DCM) and tetrahydrofuran (THF) exhibited relatively large standard deviation. The extraction of >60% of the soluble fraction was lengthy, and DCM and THF are highly volatile, with boiling points of 39.6 and 66 °C, respectively. Therefore, a considerable amount of solvent volatilized, resulting in a large error range.

Pitch (10 g) was dispersed in 500 ml hexane, acetone, toluene, and NMP for 30 min using sonication, and the samples were stirred for 2 h at a temperature below the boiling point of the respective solvent. The solutions were extracted using a Buchner funnel with a filter and an aspirator until the filtered solvent was colorless. The filtered solution was dried to evaporate the solvent, and the obtained powder was named as hexane-soluble (HS), acetone-soluble (AS), toluene-soluble (TS), and NMP-soluble (NS).

Spherical natural graphite with a particle size D_{50} of 13 μm was used to prepare the molecular weight-controlled pitch-coated graphite. To prepare pitch-coated graphite, 0.25 g of a molecular weight-controlled pitch was dispersed in 100 ml NMP for 10 min using sonication. Subsequently, 5 g graphite was added to the solution to form a homogeneous suspension, which was stirred for 1 h. The solvent was then dried using an evaporator under vacuum with continuous stirring. The as-obtained powder was carbonized at 1,300 °C for 1 h [31]. The pitch-coated graphite samples were named GHS, GAS, GTS, and GNS, depending on the pitch used. For example, GHS refers to the HS-coated graphite. The coating-free graphite was denoted as G.

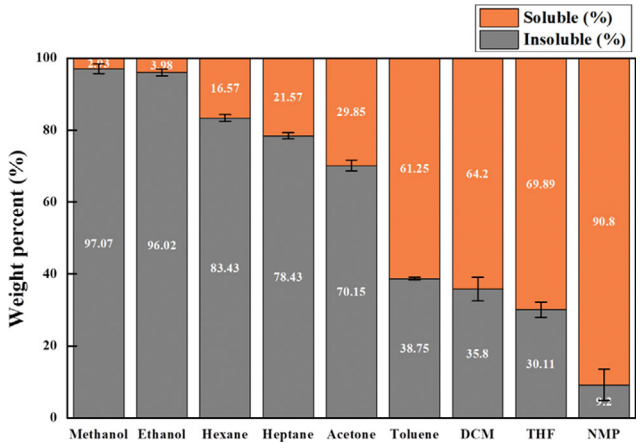

Fig. 1. Solvent fractionation percentage of pristine pitch.

2. Characterization

Matrix-assisted laser desorption ionization-time of flight mass spectrometry (MALDI-TOF-MS, Bruker Autoflex Speed TOF/TOF) was used to analyze the molecular weight distribution of the prepared pitch over a range of 0-2,000 m/z. The matrix used was 7,7,8,8-tetracyanoquinodimethane (TCNQ). Pitch is mainly composed of PAHs, and TCNQ is particularly suitable for these PAHs because of the desorption of intact PAHs and their ionization by accelerating the formation of radical cations; therefore, highly resolved mass spectra with no fragmentation or aggregation of ions were obtained [32]. Pristine pitch and NS were investigated using the water-spotting method (solvent-free method) because not all the components of NS and pristine pitch were dissolved in THF [27,33]. The HS, AS, and TS samples dissolved in THF were analyzed using the solvent method.

The carbon yield and thermal stability of the prepared pitch were characterized using TGA. Elemental analysis (EA; Thermo Scientific FLASH EA-2000 organic elemental analyzer) was used to measure the carbon, hydrogen, nitrogen, and sulfur contents of the prepared pitch.

The surface morphology of the pitch-coated graphite was analyzed using SEM (Tescan Mira 3 LMU FEG) and transmission electron microscopy (TEM).

3. Electrochemical Tests

The electrochemical performance of the coated graphite was estimated using 2032-coin cells with two electrodes. Lithium metal was used as the counter electrode and the working electrode was prepared by mixing 95 wt% prepared sample with 2.5 wt% styrene butadiene rubber and 2.5 wt% carboxyl methyl cellulose in distilled water. After mixing with a Thinky mixer, the slurry was coated onto a copper current collector and dried in a vacuum oven at 120 °C for 8 h. The loading level was typically approximately 6.5 mg cm^{-2}. The slurry was then pressed in a roll-type mill to enable a porosity of approximately 28%. Cell assembly was conducted in a glove box in an argon atmosphere to remove the effects of moisture and oxygen. The electrolyte consisted of 1 M $LiPF_6$ dissolved in a mixture of ethylene carbonate and diethyl carbonate (1 : 1 v/v). Electrochemical behavior analysis was conducted after aging for 24 h to allow sufficient electrolyte contact with the active material of the fabricated cell. Galvanostatic charge and discharge tests were performed in the potential range of 0.01-1.5 V versus Li/Li^+ at room temperature. To confirm the rate performance, lithium intercalation was performed at 0.1 C (1 C=372 mAg^{-1}), and deintercalation was performed at various rates of 0.2-5 C. Electrochemical impedance spectroscopy (EIS) was performed at an amplitude of 10 mV, frequency range of 100 kHz to 0.01 Hz, and voltage <0.7 V.

RESULTS AND DISCUSSION

1. Characterization of the Molecular Weight-controlled Pitch

1-1. Molecular Range of the Molecular Weight-controlled Pitch

The molecular weight range of the prepared pitch was exam-

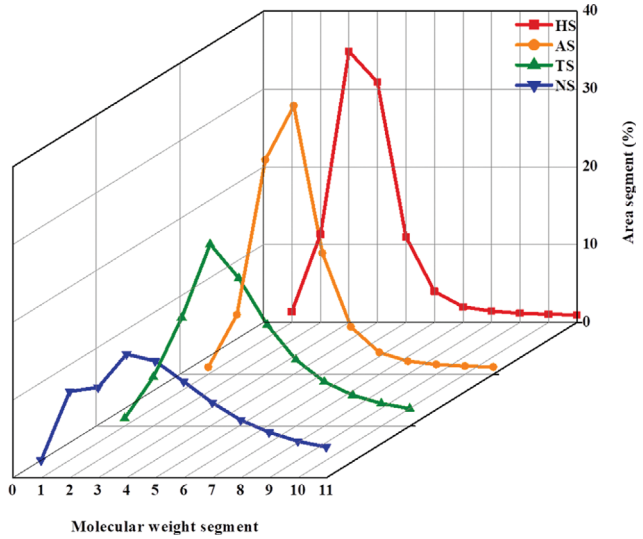

Fig. 2. Segments of molecular weight-controlled pitch based on the MALDI-TOF results.

ined using MALDI-TOF and EA. Fig. 2 shows the molecular segments of the pristine and molecular weight-controlled pitches based on the MALDI-TOF results (Fig. S1). The HS sample exhibited the lowest average molecular range, which gradually increased in the order of AS>TS>NS. Based on the MALDI-TOF results, the molecular-weight range was divided into segments and converted into percentages. Using the molecular weight of the pseudo component naphthalene, the segments were divided as follows [33]: segment 1 (100-128 m/z), segment 2 (128-256 m/z), segment 3 (256-384 m/z), segment 4 (384-512 m/z), segment 5 (512-640 m/z), segment 6 (640-768 m/z), segment 7 (768-896 m/z), segment 8 (896-1,024 m/z), segment 9 (1,024-1,152 m/z), segment 10 (1,152-1,280 m/z), and segment 11 (1,280-1,480 m/z). Segments 2-6, which represent relatively light molecular weight ranges, for HS, AS, TS, and NS were 92.03, 91.39, 75.64, and 66.08%, respectively, indicating that the light molecular weight range gradually decreased. In contrast, segments 10-11, which represent the relatively heavy molecular weight ranges, for HS, AS, TS, and NS increased by 1.99, 1.96, 5.15, and 8.70%, respectively.

Table 1 lists the elemental compositions of carbon and hydrogen as determined using EA. The H/C atomic ratio can be calculated using the carbon and hydrogen contents, which are related to the molecular weight of the pitch. The lower the H/C ratio of the prepared pitch, the higher the degree of aromatic condensation, which means that the pitch has a heavier molecular weight [34].

Table 1. Elemental contents and H/C atomic ratio of pristine and molecular weight-controlled pitch

	C (%)	H (%)	N (%)	S (%)	H/C ratio
Pristine pitch	93.39	5.45	0.12	0.09	0.70
HS	89.78	6.67	0.12	0.10	0.88
AS	91.76	6.24	0.16	0.09	0.81
TS	91.71	6.01	0.13	0.07	0.78
NS	89.02	5.69	1.73	0.08	0.76

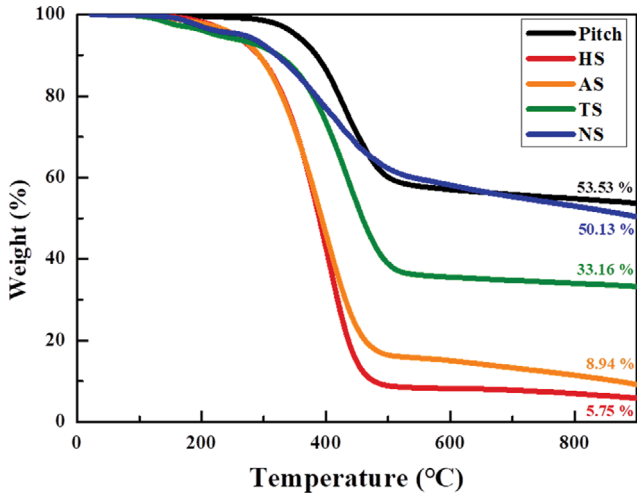

Fig. 3. TGA curve and carbon yield of pristine and molecular weight-controlled pitches.

The H/C ratio of the prepared pitch decreased in the following order: HS>AS>TS>NS. This indicates that many components with high molecular weights were present in the order of HS, AS, TS, and NS.

1-2. Thermal Analysis of the Molecular Weight-controlled Pitch

Fig. 3 shows the TGA graphs of HS, AS, TS, and NS in a nitrogen atmosphere, which can be used to examine the carbon yield and thermal stability. The amounts of residue for HS, AS, TS, and NS at 900 °C were 5.75, 8.94, 33.16, and 50.13 wt%, respectively. The mass loss started at approximately 200 °C, and the residual mass remained constant above 450 °C. HS, which consists mostly of lightweight components, exhibited the lowest carbon yield, which increases its surface roughness owing to the formation of defects in the carbon coating layer during heat treatment [35]. Conversely, the TS and NS coatings, which contained heavy molecular weight components, exhibited an increased electrochemical performance, such as a good initial Coulombic efficiency and high power rate, after being used as a coating because they were less volatile and formed a uniform coating layer. Furthermore, TS and NS, as compared to those of other carbon sources, increased the mechanical strength and electrical conductivity of the sample [36].

2. Characterization of the Molecular Weight-controlled Pitch-coated Graphite

2-1. Surface of the Molecular Weight-controlled Pitch-coated Graphite

SEM and TEM analyses were performed to investigate the surface morphology of the pitch-coated graphite, as shown in Fig. 4. The roughness of the prepared samples was estimated from the standard deviations of the SEM images. The surfaces of GHS and GAS, as compared with that of the pristine graphite (G), were rougher, and those of GTS and GNS were more uniform and had reduced roughness. Furthermore, the roughness and thickness of the surface coating layers were compared using the TEM images in Fig. 5. GHS, in which the HS coating was in the light molecular weight range, exhibited an increased surface roughness owing to the loss of volatile components during heat treatment. In contrast, GTS and GNS exhibited uniform surfaces and thickness differences. Furthermore, the coating layers of GNS, as compared with

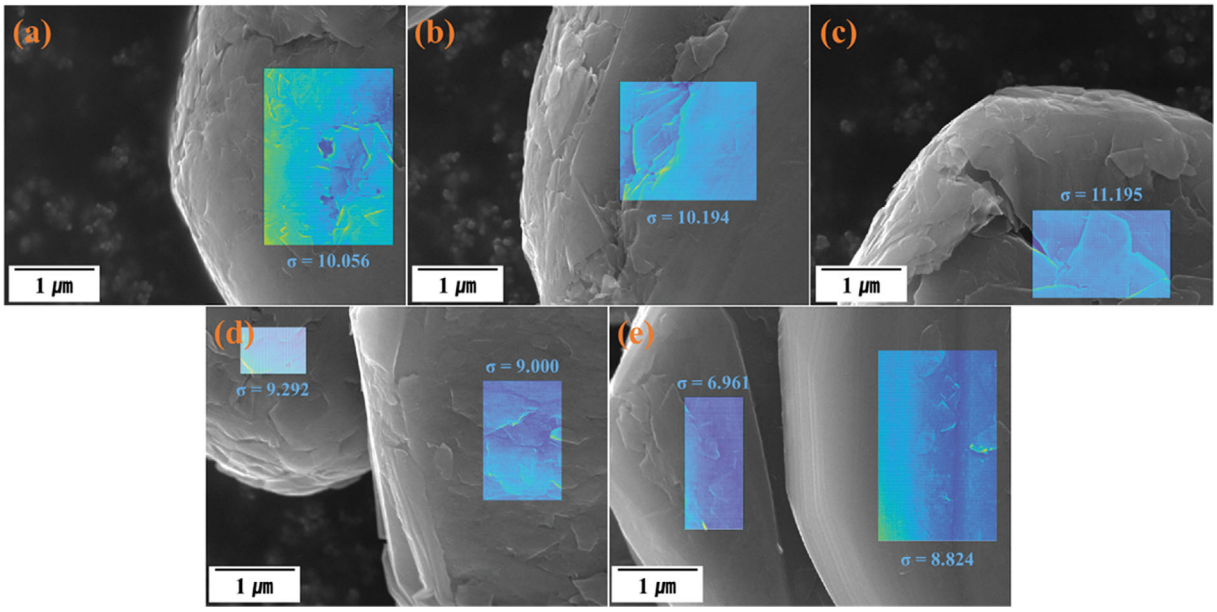

Fig. 4. SEM images of pitch-coated graphite. (a) G, (b) HS-coated graphite (GHS), (c) AS-coated graphite (GAS), (d) TS-coated graphite (GTS), and (e) NS-coated graphite (GNS).

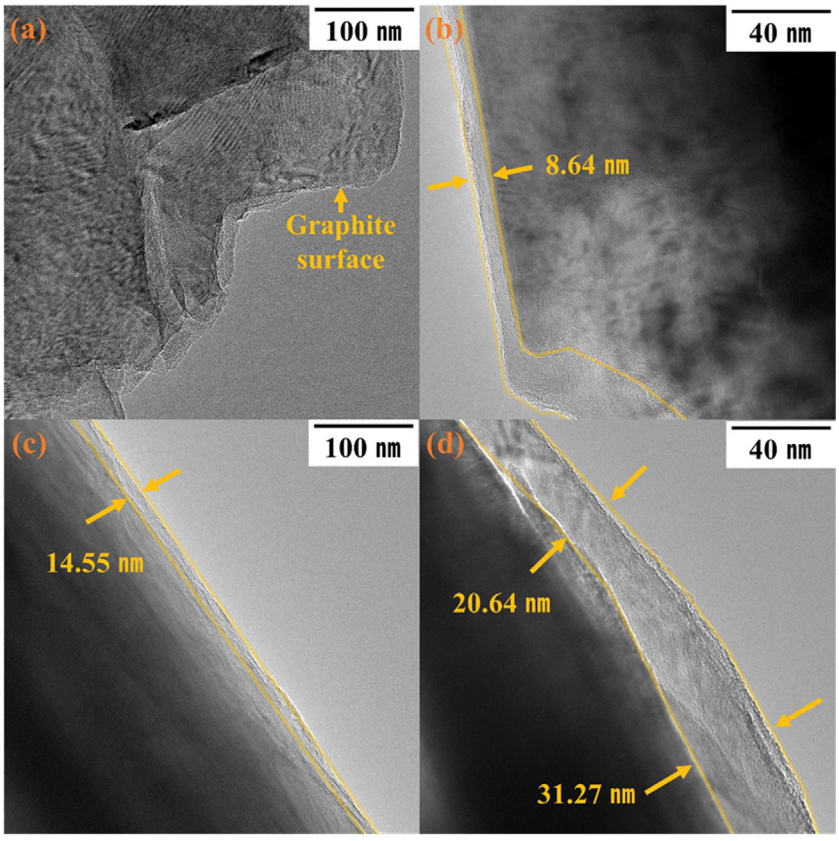

Fig. 5. TEM images of pitch-coated graphite. (a) GHS, (b) GAS, (c) GTS, and (d) GNS.

that of GTS, were thicker because of the higher carbon yield. The formation of a coating layer increased the roughness when the carbon yield of the coating pitch, which was mostly composed of light molecular weight particles, was low. In contrast, when the carbon yield of the coating pitch was high, meaning that it was composed mostly of heavy molecular weight particles, a uniform surface layer was formed and the coating thickness increased according to the carbon yield.

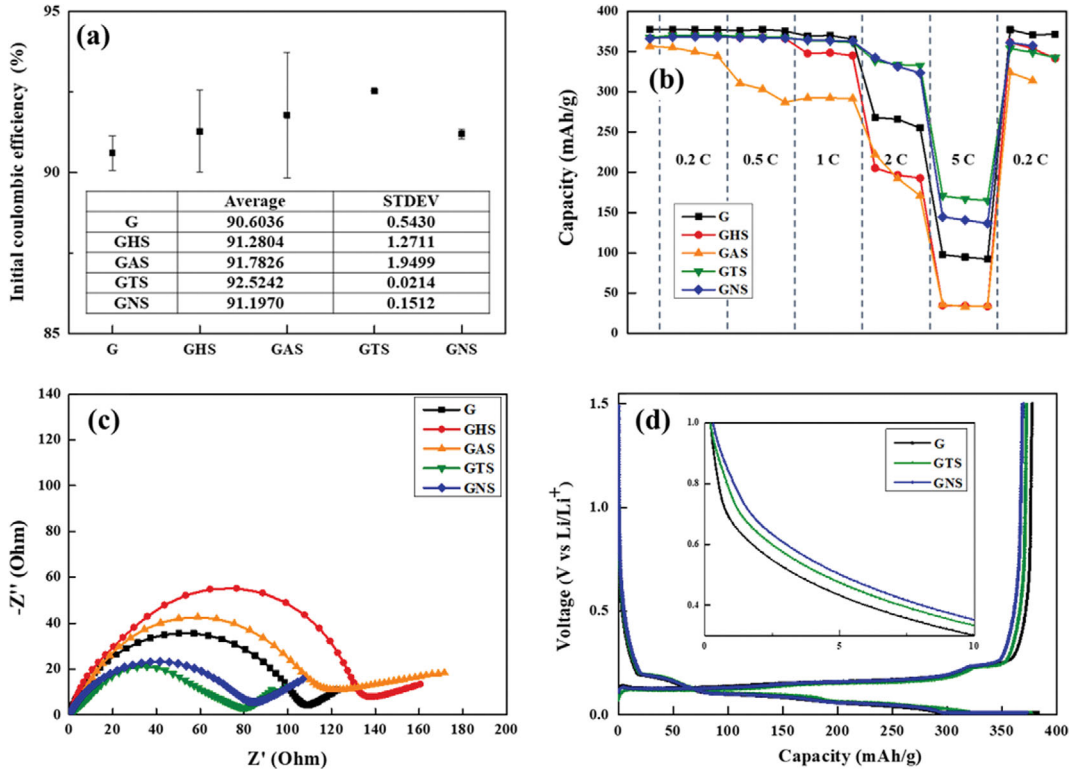

Fig. 6. Electrochemical performance of the prepared samples. (a) Initial Coulombic efficiency for G, GHS, GAS, GTS, and GNS with error bars. (b) Rate performance of G, GHS, GAS, GTS, and GNS at various delithiation rates. (c) Nyquist plots for the pitch-coated graphite after cycling. (d) Charge/discharge curves of G, GTS, and GNS at the 2nd cycle.

3. Electrochemical Performance of Pitch-coated Graphite

3-1. Initial Coulombic Efficiency

Fig. 6(a) shows the average and error bars of the initial Coulombic efficiencies of the prepared samples. The graphite surface induced the formation of an SEI layer during the first lithium intercalation process, resulting in a decrease in the reversible capacity [37]. Therefore, G exhibited the lowest initial coulombic efficiency of 90.60%. All the pitch-coated graphite samples exhibited increased initial Coulombic efficiency because the formation of a coating layer prevented direct contact between the pitch-coated graphite electrode and the electrolyte, thereby reducing the SEI layer formation and increasing the initial coulombic efficiency [24]. However, the error bar ranges for GHS and GAS were 1.27 and 1.95, respectively, which were larger than those for GTS and GNS, owing to their low carbon yield. A low carbon yield indicates that the roughness of the coating layer increases because of the volatilization of light molecular components during heat treatment; therefore, a low carbon yield is attributed to nonuniform surfaces and surface defects [35]. This is consistent with the SEM images shown in Fig. 4. GTS and GNS exhibited error bars of 0.02, and 0.15, respectively, indicating the high thermal stability of TS and NS, resulting in a homogeneous surface for each particle in the sample. Therefore, these samples exhibited a very low variance and increased initial efficiency. In particular, GTS exhibited little difference in its error bars, making it the optimal molecular weight range for the coating pitch.

3-2. Rate Performance and EIS

The rate performance was determined to investigate the discharge capacity based on the rate of the prepared samples, as shown in Fig. 6(b). Charge (Li^+ intercalation) was performed in the constant current/constant voltage mode at 0.1 C for only the first cycle, and then at 0.2 C. Discharge (Li^+ deintercalation) was performed in the CC mode at different rates from 0.2 C to 5 C to confirm the rate capability (5 C/0.2 C). Here, the 1 C rate was equal to the graphite theoretical capacity of 372 mA g^{-1}. The 5 C/0.2 C rate capability of GTS (46.12%) and GNS (39.33%) were higher than that of G (25.87%). From a microscopic perspective, graphite has an anisotropic structure consisting of edge and basal planes. Most lithium ions are intercalated/deintercalated through the edge plane of graphite; however, the basal plane of graphite has difficulty intercalating/deintercalating lithium ions. Therefore, the rate capability of graphite is limited, but can be improved by forming an isotropic carbon coating on its surface [25]. The coating layer consisted of amorphous carbon with an isotropic structure. This isotropic structure consisted of randomly oriented hexagonal rings or graphene sheets. The anisotropic carbon coating forms equivalent diffusion paths for lithium ions; therefore, the rate performance of GTS and GNS increased with a uniform coating layer. However, GHS and GAS were confirmed to have poorer rate performance (9.39 and 10.09%, respectively) than G (25.87%). As mentioned above, owing to the relatively nonuniform and high roughness of the GHS and GAS surfaces, the coating layer increased the resistance of the material, thereby suppressing the rate performance.

As shown in Fig. 6(c), the semicircle in the EIS results clearly confirms that the charge transfer resistance (Rct) of GHS (138.68 Ω)

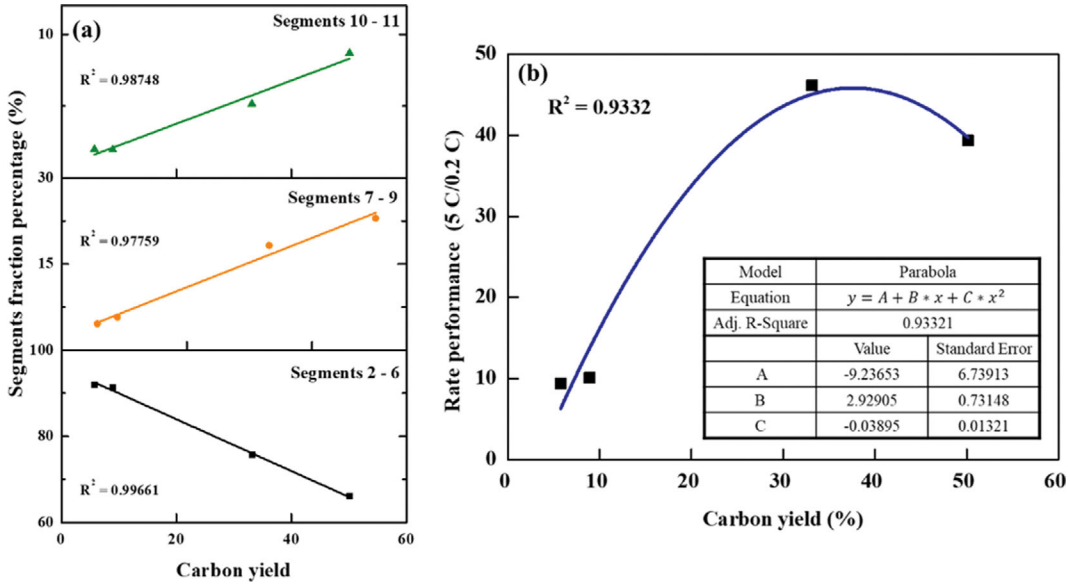

Fig. 7. Correlation between the properties of coating pitch and the rate performance of coated graphite anodes. (a) Carbon yield as a function of the segment fraction percentage. (b) Carbon yield as a function of the rate performance.

and GAS (123.84 Ω) increased, as compared to that of G (108.83 Ω). The Rct at the electrode/electrolyte interface indicates the kinetics of the electrochemical reaction and can change based on the carbon coating, surface modification, electrolyte additives, and other factors [38,39]. A larger Rct value indicates that it is difficult to intercalate/deintercalate lithium ions. Therefore, the non-uniform surfaces and surface defects of GHS and GAS hindered lithium-ion intercalation/deintercalation. The Rct values of GTS (79.84 Ω) and GNS (86.82 Ω) were lower than that of graphite because of the uniform surface of the isotropic carbon-coating layer.

In particular, the rate properties of GTS, as compared with those of GNS, were improved owing to the high carbon yield of NS, which increased the coating thickness. Fig. 6(d) shows the charge-discharge curves of the second cycle of G, GTS, and GNS. The graphite curve is steeper than that of amorphous carbon at approximately 1 V during intercalation [40]. The slope is less steep near 1 V in the order G>GTS>GNS, indicating that the coating layer of GNS is thicker than that of GTS. The thick GNS coating layer increased the diffusion path length of lithium ions; therefore, this coating layer increased the resistance when lithium ions were deintercalated, resulting in a poor rate performance.

3-3. Correlations Between the Molecular Range, Electrochemical Properties, and Structure Design of Pitch-coated Graphite

Considering these results, the coating effect and surface formed varied according to the molecular weight range, indicating that they were significantly influenced by the carbon yield. Therefore, to examine the molecular weight range and electrochemical properties, the correlation between the carbon yield and each molecular weight range was first investigated and then the correlation between the molecular weight range and electrochemical properties was determined. Based on these results, the structure of pitch-coated graphite was investigated.

The correlation between the carbon yield and electrochemical performance was confirmed based on the TGA and MALDI-TOF mass spectrometry results. Fig. 7(a) shows a plot of the carbon yields and segments. The segment division criteria were HS, HI-TS, and TI-NMPS, which can be seen in Fig. S1 and Table S1. Segments 2-6 represent a relatively light molecular weight range, whereas segments 10-11 represent a heavy molecular weight range. The determination coefficients of each graph are all 0.95 or higher, indicating that the given linear behavior is suitable. That is, each segment and the carbon yield exhibits a linear relationship. The electrochemical performance of pitch-coated graphite was significantly altered by the surface morphology after coating and heat treatment, and these variations were associated with the carbon yield. Fig. 7(b) shows a graph of the carbon yield and rate performance. The most improved rate performance occurred when the carbon yield was approximately 30, which then decreased. Notably, this graph exhibits a reliable relationship with a determination coefficient of 0.93. The carbon yield, segment graphs, and rate performance graphs exhibit reliable correlations, indicating that the correlation between the segments and rate performance is dependable.

Fig. 8 shows the dependence of the rate performance on the segment fraction, which can be divided into the following four regions depending on the rate performance.

(1) The "A" region, which includes GHS and GAS, exhibited poorer electrochemical performance than uncoated G. A larger fraction of segments 2-6 results in more surface defects and a higher roughness, as shown in Figs. 4 and S2. The formation of this surface led to poor electrochemical performance, with a smaller fraction of segments 2-6 facilitating the formation of homogeneous surfaces. However, a small amount of light molecular components indicates an increase in viscosity [41]; therefore, the pitch easily aggregated during the coating process. In summary, under the described experimental conditions, the use of a coating pitch consisting of approximately 70-84.49% of segments 2-6 is recommended.

(2) The region where the electrochemical performance began to improve after coating was "B," and the peaks in region "C". That

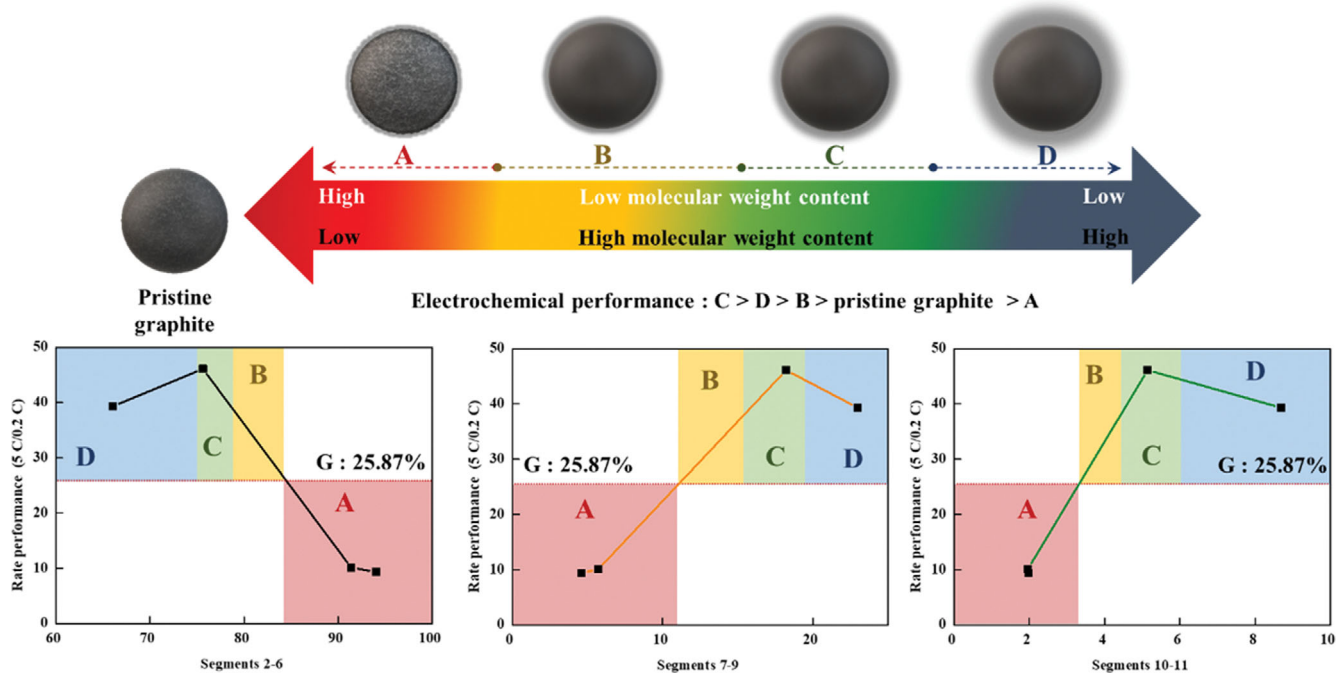

Fig. 8. Rate performance as a function of the molecular weight fraction of coated pitch. A: GHS, B: GAS, C: GTS, and D: GNS.

is, the electrochemical performance increased continuously from 11.20 to 18.21% for segments 7-9, and from 3.35 to 5.15% for segments 10-11. However, their electrochemical properties deteriorated. The reason for this difference in the properties is the formation of a homogeneous surface and an appropriate coating thickness. Therefore, the "C" region formed a surface without defects, which made the uniform coating layer not excessively thick, resulting in an outstanding rate performance. In particular, 18.21% of segments 7-9 and 5.15% of segments 10-11 exhibited the best molecular weight distribution for the coating pitch.

(3) The "D" region included the GNS sample, which contained the highest content of segments 10-11. It is noteworthy that the heavy molecular weight range did not necessarily improve the electrochemical properties; rather, the coating layer became excessively thick, which increased the charge transfer resistance and caused the characteristics to deteriorate. Furthermore, with regard to other parameters, such as the coating ratio, solution concentration, and heat-treatment temperature, the electrochemical properties can be improved by controlling the coating thickness.

Based on these results, the structural design of the pitch-coated graphite according to the molecular weight range is shown in the upper part of Fig. 8. In summary, 128-768 m/z, which is the lighter fraction of pitch, assists in forming a homogeneous surface by decreasing the viscosity during carbonization. The heavier fraction, 768-1,480 m/z, was the main component that formed the coating layer. This improved the rate performance of the anode by forming an isotropic layer, which increased the number of lithium-ion intercalation sites. However, a thick surface increases the charge-transfer resistance because of the increased diffusion path lengths of lithium ions. Therefore, the pitch molecular weight fractions of 128-768, 768-1,152, and 1,152-1,480 m/z should be controlled to 70-84.49, 11.20-18.21, and 3.35-5.15%, respectively.

CONCLUSIONS

The effects of the molecular weight range of coating pitch on the electrochemical performance were investigated. The molecular weight range was divided into three regions based on the MALDI-TOF results, with segments 2-6, 7-9, and 10-11 representing the light, medium, and heavy molecular weight ranges, respectively. GHS and GAS, containing 85% or more of segments 2-6, exhibited a heterogeneous coating surface owing to the loss of a large number of volatile components during heat treatment, resulting in an inconsistent initial efficiency and reduced rate performance. Notably, the coating pitch with a lower content (approximately 85%) of segments 2-6 formed a uniform surface, which improved the electrochemical properties, and the coating pitch with segments 7-9 and 11-12 contents>11.20 and 33.35%, respectively, enhanced the electrochemical performance. The 5 C/0.2 C capacitance of GTS was 46.12%, as compared to the 25.87% of G. However, an excess content of segments 7-11 resulted in poor electrochemical properties because the formation of a thick coating layer increased the charge transfer resistance and hindered lithium diffusion resistance. In summary, the best electrochemical properties were observed for 18.21% of segments 7-9 and 5.15% of segments 10-11; these molecular weight ranges were thought to be optimal for coating pitch.

ACKNOWLEDGEMENTS

This study was supported by the Technology Innovation Program (20007171, Development of artificial graphite from cokes and binder/coating pitch for anode materials) funded by the Min-

istry of Trade, Industry, and Energy (MOTIE, Korea) and by the Technology Innovation Program (20006696, Development of isotropic graphite block for semiconductor process) funded by the Ministry of Trade, Industry, and Energy (MOTIE, Korea).

SUPPORTING INFORMATION

Additional information as noted in the text. This information is available via the Internet at http://www.springer.com/chemistry/journal/11814.

REFERENCES

1. M. S. Javed, A. Mateen, I. Hussain, A. Ahmad, M. Mubashir, S. Khan, M. A. Assiri, S. M. Eldin, S. S. A. Shah and W. Han, *Energy Storage Mater.*, **53**, 827 (2022).
2. M. S. Javed, A. Mateen, S. Ali, X. Zhang, I. Hussain, M. Imran, S. S. A. Shah and W. Han, *Small*, **18**, 2201989 (2022).
3. Q. Zhang, S. Wang, Y. Liu, M. Wang, R. Chen, Z. Zhu, X. Qiu, S. Xu and T. Wei, *Energy Technol.*, **11**, 2201438 (2023).
4. J. Lu, Z. Wang, Q. Zhang, C. Sun, Y. Zhou, S. Wang, X. Qiu, S. Xu, R. Chen and T. Wei, *Chin. J. Chem. Eng.*, **60**, 80 (2023).
5. X. Zhang, Y. Tang, F. Zhang and C.-S. Lee, *Adv. Energy Mater.*, **6**, 1502588 (2016).
6. S. Mu, Q. Liu, P. Kidkhunthod, X. Zhou, W. Wang and Y. Tang, *Natl. Sci. Rev.*, **8**, nwaa178 (2021).
7. C. Ma, Y. Zhao, J. Li, Y. Song, J. Shi, Q. Guo and L. Liu, *Carbon*, **64**, 553 (2013).
8. Y. Hai, W. Cui, Y. Lin, P. Han, H. Chen, Z. Zhu, C. Li, B. Yang, C. Zhu and J. Xu, *Appl. Surf. Sci.*, **484**, 726 (2019).
9. L. Zhao, B. Ding, X.-Y. Qin, Z. Wang, W. Lv, Y.-B. He, Q.-H. Yang and F. Kang, *Adv. Mater.*, **34**, 2106704 (2022).
10. W. He, T. Zhang, J. Jiang, C. Chen, Y. Zhang, N. Liu, H. Dou and X. Zhang, *ACS Appl. Energ. Mater.*, **3**, 4394 (2020).
11. Y. Yang, W. Shi, R. Zhang, C. Luan, Q. Zeng, C. Wang, S. Li, Z. Huang, H. Liao and X. Ji, *Electrochim. Acta*, **204**, 100 (2016).
12. T. Tsumura, A. Katanosaka, I. Souma, T. Ono, Y. Aihara, J. Kuratomi and M. Inagaki, *Solid State Ion.*, **135**, 209 (2000).
13. T. Placke, V. Siozios, R. Schmitz, S. F. Lux, P. Bieker, C. Colle, H.-W. Meyer, S. Passerini and M. Winter, *J. Power Sources*, **200**, 83 (2012).
14. H.-H. Chen, V. Goel, M. J. Namkoong, M. Wied, S. Müller, V. Wood, J. Sakamoto, K. Thornton and N. P. Dasqupta, *Adv. Energy Mater.*, **11**, 2003336 (2021).
15. Y. Shen, X. Shen, M. Yang, J. Qian, Y. Cao, H. Yang, Y. Luo and X. Ai, *Adv. Funct. Mater.*, **31**, 2101181 (2021).
16. Y. Mu, M. Han, J. Li, J. Liang and J. Yu, *Carbon*, **173**, 477 (2021).
17. H. Yu, Y. Chen, W. Wei, X. Ji and L. Chen, *ACS Nano*, **16**, 9736 (2022).
18. M. Yoshio, H. Wang, K. Fukuda, Y. Hara and Y. Adachi, *J. Electrochem. Soc.*, **147**, 1245 (2000).
19. H.-Y. Lee, J.-K. Baek, S.-M. Lee, H.-K. Park, K.-Y. Lee and M.-H. Kim, *J. Power Sources*, **128**, 61 (2004).
20. Y. Gao, J. Zhang, Y. Chen and C. Wang, *Surf. Interfaces*, **24**, 101089 (2021).
21. H. Wang, Y. Chen, H. Yu, W. Liu, G. Kuang, L. Mei, Z. Wu, W. Wei, X. Ji, B. Qu and L. Chen, *Adv. Funct. Mater.*, **32**, 2205600 (2022).
22. R. C. Shurtz, J. D. Engerer and J. C. Hewson, *J. Electrochem. Soc.*, **165**, A3891 (2018).
23. F. Béguin, F. Chevallier, C. Vix-Guterl, S. Saadallah, V. Bertagna, J. N. Rouzaud and E. Frackowiak, *Carbon*, **43**, 2160 (2005).
24. Y. F. Zhou, S. Xie and C. H. Chen, *Electrochim. Acta*, **50**, 4728 (2005).
25. C. Wang, H. Zhao, J. Wang, J. Wang and P. Lv, *Ionics*, **19**, 221 (2012).
26. B.-H. Kim, J.-H. Kim, J.-G. Kim, M.-J. Bae, J.-S. Im, C.-W. Lee and S. Kim, *J. Ind. Eng. Chem.* **41**, 1 (2016).
27. J. G. Kim, J. H. Kim, B.-J. Song, C. W. Lee and J. S. Im, *J. Ind. Eng. Chem.*, **36**, 293 (2016).
28. Y. J. Han, J. U. Hwang, K. S. Kim, J. H. Kim, J. D. Lee and J. S. Im, *J. Ind. Eng. Chem.*, **73**, 241 (2019).
29. B. C. Bai, J. G. Kim, J. H. Kim, C. W. Lee, Y.-S. Lee and J. S. Im, *Carbon Lett.*, **25**, 78 (2018).
30. B.-H. Kim, J.-H. Kim, J.-G. Kim, J. S. Im, C. W. Lee and S. Kim, *J. Ind. Eng. Chem.*, **45**, 99 (2017).
31. T. K. Whang, J. H. Kim, J. S. Im and S. C. Kang, *Appl. Chem. Eng.*, **32**(1), 83 (2021).
32. W. F. Edwards, L. Jin and M. C. Thies, *Carbon*, **41**, 2761 (2003).
33. J. H. Kim, Y. J. Choi, J. S. Im, A. Jo, K. B. Lee and B. C. Bai, *J. Ind. Eng. Chem.*, **88**, 251 (2020).
34. W. Zhang, J. T. Andersson, H. J. Räder and K. Müllen, *Carbon*, **95**, 672 (2015).
35. Y.-J. Han, J. Kim, J.-S. Yeo, J. C. An, I.-P. Hong, K. Nakabayashi, J. Miyawaki, J.-D. Jun and S.-H. Yoon, *Carbon*, **94**, 432 (2015).
36. S.-H. Choi, G. Nam, S. Chae, D. Kim, N. Kim, W. S. Kim, J. Ma, J. Sung, S. M. Han, M. Ko, H.-W. Lee and J. Cho, *Adv. Energy Mater.*, **9**, 1803121 (2019).
37. L. Chan, Q. Qu, L. Zhang, M. Shen, L. Zhang and H. Zheng, *Electrochim. Acta*, **105**, 378 (2013).
38. R. Yazami and Y. F. Reynier, *Electrochim. Acta*, **47**, 1217 (2002).
39. X. Gong, J. Zheng, Y. Zheng, S. Cao, H. Wen, B. Lin and Y. Sun, *Electrochim. Acta*, **356**, 136858 (2020).
40. J. R. Dahn, T. Zheng, Y. Liu and J. S. Xue, *Science*, **270**, 590 (1995).
41. W. Jiang, G. Ni, P. Zuo, S. Qu, Y. Li, H. Niu and W. Shen, *Carbon Lett.*, **29**, 505 (2019).